Earth and Planetary Science Letters 288 (2009) 539–550

Contents lists available at ScienceDirect

Earth and Planetary Science Letters

journal homepage: www.elsevier.com/locate/epsl

Magnetostratigraphy of the Dahonggou section, northern Qaidam Basin and its bearing on Cenozoic tectonic evolution of the Qilian Shan and Altyn Tagh Fault

Haijian Lu *, Shangfa Xiong

Key Laboratory of Cenozoic Geology and Environment, Institute of Geology and Geophysics, Chinese Academy of Sciences, Beijing 100029, China

ARTICLE INFO

Article history:
Received 2 May 2009
Received in revised form 7 August 2009
Accepted 12 October 2009
Available online 10 November 2009

Editor: T.M. Harrison

Keywords:
Qilian Shan
Altyn Tagh Fault
tectonic uplift
magnetostratigraphy
Dahonggou section

ABSTRACT

The timing of uplift of the Tibet Plateau has a central role in the development of tectonic models for the Tibet Plateau and Cenozoic global climate change. A detailed magnetostratigraphic study of the Dahonggou section, northern Qaidam Basin, reveal that the section spans from ~34 to ~8.5 Ma and the ages of the Shang Ganchaigou, Xia Youshashan and Shang Youshashan formations are from >34 to 22–20 Ma, 22–20 to 13 Ma and 13 to <8.5 Ma, respectively. Variations in lithofacies, sedimentation rate and magnetic susceptibility (K) suggest that the southern Qilian Shan was tectonically inactive and didn't respond to the rapid slip on the Altyn Tagh Fault at 30 Ma. In contrast, the similar sedimentary records in the Dahonggou section, the Xishuigou section along the Altyn Tagh Fault, and even more localities along much of the Qilian range front imply that the Qilian Shan and the Altyn Tagh Fault were synchronously tectonically active at about 12 Ma. The lower K between ~12 Ma and ~8.5 Ma in the sediments of the Dahonggou section is interpreted to be due to long-distanced oxidation and sorting, which cause not only that magnetite was oxidated to hematite, but also that magnetic minerals are enriched in fine-grained sediments and coarse-grained sediments bear few magnetic mineral.

1. Introduction

The timing and nature of the uplift of the Tibetan Plateau have recently been a focus of not only tectonic geologists, but also paleoclimatic geologists who prefer to link late Cenozoic regional and global climate changes with the uplift of the Tibetan Plateau. A variety of tectonic mechanisms for the uplift of the Tibetan Plateau has been proposed during the last several decades (e.g., Harrison et al., 1992; England and Houseman, 1989; Molnar et al., 1993). These models can be classified into three categories according to Harrison et al. (1998), namely, the wholesale uplift models, the progressive growth models and the inherited plateau models. Given the complexity of the tectonic history, it seems that different mechanisms may have operated at various periods of time since the India–Asia collision. Recently, in the 'stepwise-diachronous rise' model, the northern Tibet is assigned to be 'Pliocene–Quaternary Tibet' and assumed to be uplifted since the late Miocene (Tapponnier et al., 2001), although better constraints of the timing of the uplift of this region require more works, including high resolution magnetostratigraphic measurements of the sedimentary basins on the periphery and interior of the northern Tibet.

An array of magnetostratigraphic works has currently been conducted within and on the margin of the northern Tibet (Fig. 1) (e.g., Li et al., 1997; Yin et al., 1998; Zheng et al., 2000; Yue et al., 2001; Zhao et al., 2001; Song et al., 2001; Gilder et al. 2001; Chen et al., 2002; Wang et al., 2003; Liu et al., 2003; Pares et al., 2003; Fang et al., 2003, 2005a,b; Sun et al., 2004, 2005a,b; Dai et al., 2005; Charreau et al., 2005, 2006; Dai et al., 2006; Huang et al., 2006; Fang et al., 2007; Heermance et al., 2007, 2008; Sun and Zhang, 2008, 2009). As the largest basin in the northeast of the Tibetan Plateau and with a maximum Cenozoic sediment thickness of ~12,000 m, the Qaidam Basin possesses an important sedimentary archive for the understanding of tectonic evolution, as well as climate change of the northern Tibetan Plateau. Previously, much work on the Cenozoic sediments of the Qaidam Basin have been undertaken and are helpful in revealing not only tectonic implications associated with the India–Asia collision (Métivier et al., 1998, 1999; Chen et al., 1999; Hanson, 1999; Rumelhart, 1999; Gilder et al., 2001; Meng et al., 2001; Yin et al., 2002; Sun et al., 2005a,b; Zhou et al., 2006; Wang et al., 2006; Zhu et al., 2006; Fang et al., 2007; Yin et al., 2008; Ritts et al., 2008; Bovet et al., 2009), but also depositional processes (Wang and Coward, 1990; Huang and Shao, 1993; Huang et al., 1996; Sun et al., 1999; Pang et al., 2004; Rieser et al., 2005; Wang et al., 2007) and inland aridification in Asia (Liu et al., 1996; Wang et al., 1999; Rieser et al., 2005) which are also tightly coupled with the tectonic uplift associated with the India–Asia collision.

However, at least two problems remained in studies on the Cenozoic sediments in the Qaidam Basin. Firstly, the time controls of many previous studies are mainly based on isotope geochronology (Zhou et al., 2006), fission track dating (Liu et al., 1996; Wang et al., 1999) and old magnetostratigraphic study (Wang et al., 1999; Sun et al., 1999; Yin et al., 2002; Zhou et al., 2006; Yin et al., 2008; Rieser et al., 2005; Wang et al., 2007) and not only disagree with one another, but also disaccord with recent magnetostratigraphic ages constrained by mammalian fossils or ostracoda assemblages (Sun et al., 2005a,b; Fang et al., 2007).

* Corresponding author. Tel.: +86 10 82998263.
E-mail address: haijianlu2007@126.com (H. Lu).

0012-821X/$ – see front matter © 2009 Elsevier B.V. All rights reserved.
doi:10.1016/j.epsl.2009.10.016

The age assignments of stratigraphy in the Qaidam Basin have remained in dispute. Secondly, compared with recent flourishing magnetostratigraphic studies in the surrounding of Tian Shan and Qilian Shan (Fig. 1), studies of the Qaidam Basin are few and of relatively short interval (Sun et al., 2005a,b; Fang et al., 2007), which limit the understanding of long-term tectonic and sedimentary evolution in the Qaidam Basin.

Here we report a magnetostratigraphic study of a ~3600 m thick and continuous composite section (the Dahonggou section) in the Qaidam Basin (Fig. 2). The results provide new evidence for constraining the timing of the tectonic evolution in the northern Tibetan Plateau.

2. Geological setting and stratigraphy

The Qaidam Basin, with an average elevation of ~3000 m, is the largest intermontane basin (covering an area of ~120,000 km^2) at the northeastern corner of the Tibetan Plateau. The basin is bordered by three large fault systems: the Kunlun thrust belt to the south, the left-lateral strike-slip Altyn Tagh Fault to the northwest and the Qilian Shan–Nan Shan thrust-and-fold belt to the northeast. Seismic reflection studies indicate that the Qaidam Basin is bounded by thrust faults along its northern and southern margins, but its center is relatively tectonically quiet (Di and Wang, 1991; Dai et al., 2003). The thrust system at the northern margin of the Qaidam Basin (Fig. 2B) is considered to form as the long-distanced response of the India–Asia collision, with the process of stepwise thrusting from northeast to southwest since Eocene to Pleistocene (Liu et al., 2005). Our study area (the Dahonggou section) is just in the thrust system of northern Qaidam Basin (Fig. 2B). Like other thrust belts, the thrust in the Dahonggou section also exhibit an L-shaped geometry (Fig. 3A). Because the lateral ramps are subparallel to the left-slip Altyn Tagh Fault, their development may result from a distributed left-slip deformation that transfers motion from the Altyn Tagh Fault to the left-slip ramps via linking thrusts (Yin et al., 2008).

Previous work by petroleum geologists over the last 50 years has established a basin-wide lithostratigraphic framework for the Qaidam Basin. The Cenozoic stratigraphy was divided into seven formations (in ascending order): Lulehe, Xia Ganchaigou, Shang Ganchaigou, Xia Youshashan, Shang Youshashan, Shizigou, and Qigequan. The Dahonggou section is a composite of section-k and section-q, starting from the lower part of Shang Ganchaigou formation, and ending just at the top of Shang Youshashan formation (Fig. 3).

The ~1390 m thick Shang Ganchaigou formation consists mainly of cyclic alternations of gray-green laminated or bedded siltstone and brown mudstone. The Xia Youshashan formation is ~1220 m thick and consists largely of alternating brown laminated or bedded mudstone and gray-green massive sandstone, or conglomerate, or multi-colored (gray-white to yellowish) siltstone. The Shang Youshashan formation is ~1000 m thick and mostly composed of interbedded yellowish massive conglomerate, sandy conglomerate, with brown or yellow massive sandstone intercalated with yellow massive siltstone. Particularly noteworthy are the discoveries of *Chilotherium*, *Cyprideis*, and *Gomphotherium* in the upper and middle part of Shang Youshashan formation and in the upper part of Xia Youshashan formation respectively, by Qinghai BGMR (1984) within our studied section (Fig. 3A). *Chilotherium* was primarily discovered in late Miocene stratigraphy (Deng et al, 2004; Deng, 2005), whereas *Gomphotherium* amply occurred during Mid-Miocene (Deng, 2004; Deng et al, 2004; Deng, 2005; Deng et al, 2007) in the northwestern China. *Cyprideis* have appeared in abundance throughout the Qaidam Basin and become a predominant Ostracoda species since 12 Ma (Yang et al., 2000).

3. Paleomagnetic sampling and analytical method

All samples were collected from section-k and section-q, which are approximately 2.5 km away from each other. Section-k is ~1320 m in thickness and consists of the Shang Youshashan formation and the upper part of the Xia Youshashan formation. Section-q spans ~2380 m

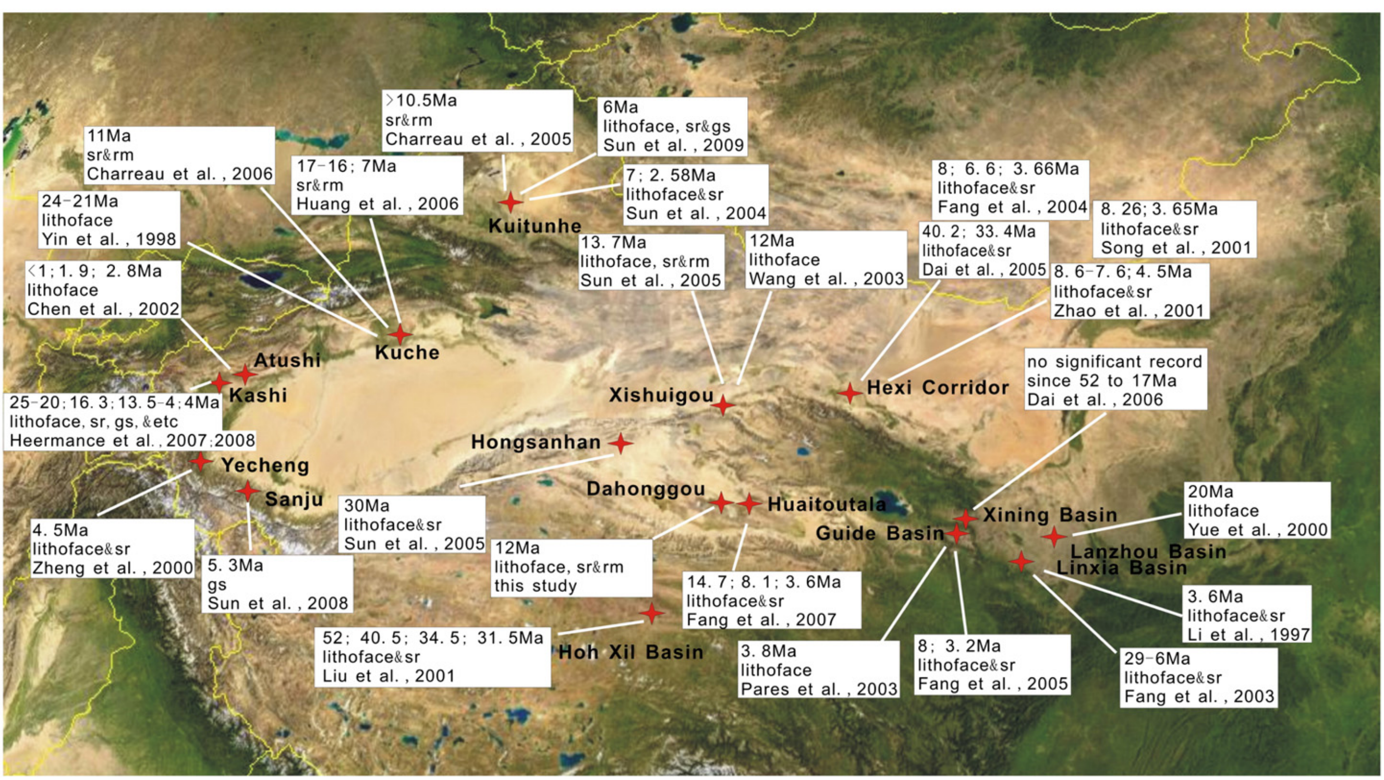

Fig. 1. The recent magnetostratigraphic studies on the northern Tibetan Plateau (Li et al., 1997; Yin et al., 1998; Zheng et al., 2000; Yue et al., 2001; Zhao et al., 2001; Song et al., 2001; Chen et al., 2002; Wang et al., 2003; Liu et al., 2003; Pares et al., 2003; Fang et al., 2003; Sun et al., 2004; Charreau et al., 2005; Fang et al., 2005a,b; Sun et al., 2005; Dai et al., 2005, 2006; Huang et al., 2006; Charreau et al., 2006; Fang et al., 2007; Heermance et al., 2007; Heermance et al., 2008; Sun and Zhang, 2008, 2009). The white rectangles note the timing and signature of tectonic uplift. The sr, rm and gs are sedimentation rate, rock magnetism and growth strata respectively.

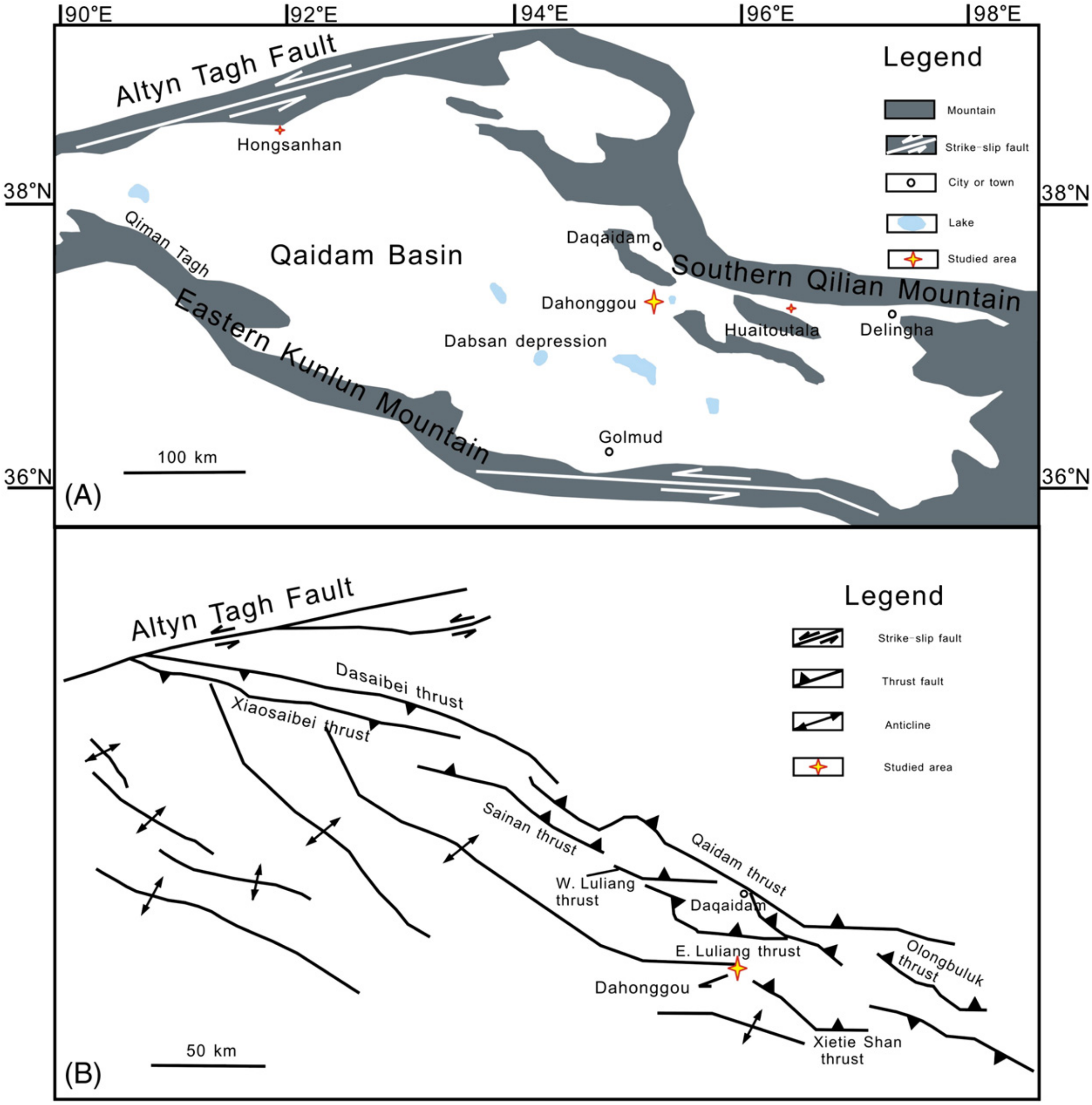

Fig. 2. A: Sketch map of the Qaidam Basin showing the locations of studied sections that are mentioned in the text. B: Present configuration of north Qaidam thrust system, modified after Yin et al., 2008.

in thickness and consists of the Shang Ganchaigou formation and a majority of the Xia Youshashan formation. The lower part of section-k and the upper part of section-q overlap lithologically with a thickness of about 100 m, and it can be readily recognized by satellite images and stratigraphic correlation in the field.

The samples were oriented with a magnetic compass in the field and collected as standard oriented hand samples. We collected fine-grained lithology as much as possible and the samples are basically mudstone, siltstone and sandstone for the entire section-q and the lower part of section-k, and siltstone and sandstone for the upper part of section-k. The average sampling interval varied from 0.5 to 5 m for the upper part of section-k (with a relatively coarse grain size) and 0.5–2 m for the section-q and the lower part of section-k depending on the lithology. In section-k, a few parts of exposures were totally washed away by floodwater, causing some gaps in the sampling. In total, 1643 block samples were collected from the two sub-sections. All samples were then taken to the laboratory where they were fashioned into 2 cm cubes for paleomagnetic measurement.

The samples were analyzed at the paleomagnetic and rock magnetic laboratory of the key laboratory of the western China's environmental system in Lanzhou University. All samples were stored, demagnetized, and measured within a magnetically shielded room with average field intensity of <300 nT. The samples were subjected to stepwise thermal demagnetization in MMTD-48 thermal demagnetizer. We first employed 19 temperature steps from 25 °C to 680 °C at intervals of 50–150 °C between 25 °C and 550 °C, and 10–25 °C above 550 °C for 344 specimens, which were evenly selected from all samples. Based on initial demagnetizations, only 11 steps were selected for the remaining specimens and comprise 25 °C, 150 °C, 300 °C, 350 °C, 400 °C, 450 °C, 500 °C, 550 °C, 600 °C, 620 °C, and 650 °C. Measurements of remanent magnetization were made with 2G-760R cryogenic magnetometer. Demagnetization results were analyzed on stereographic projections

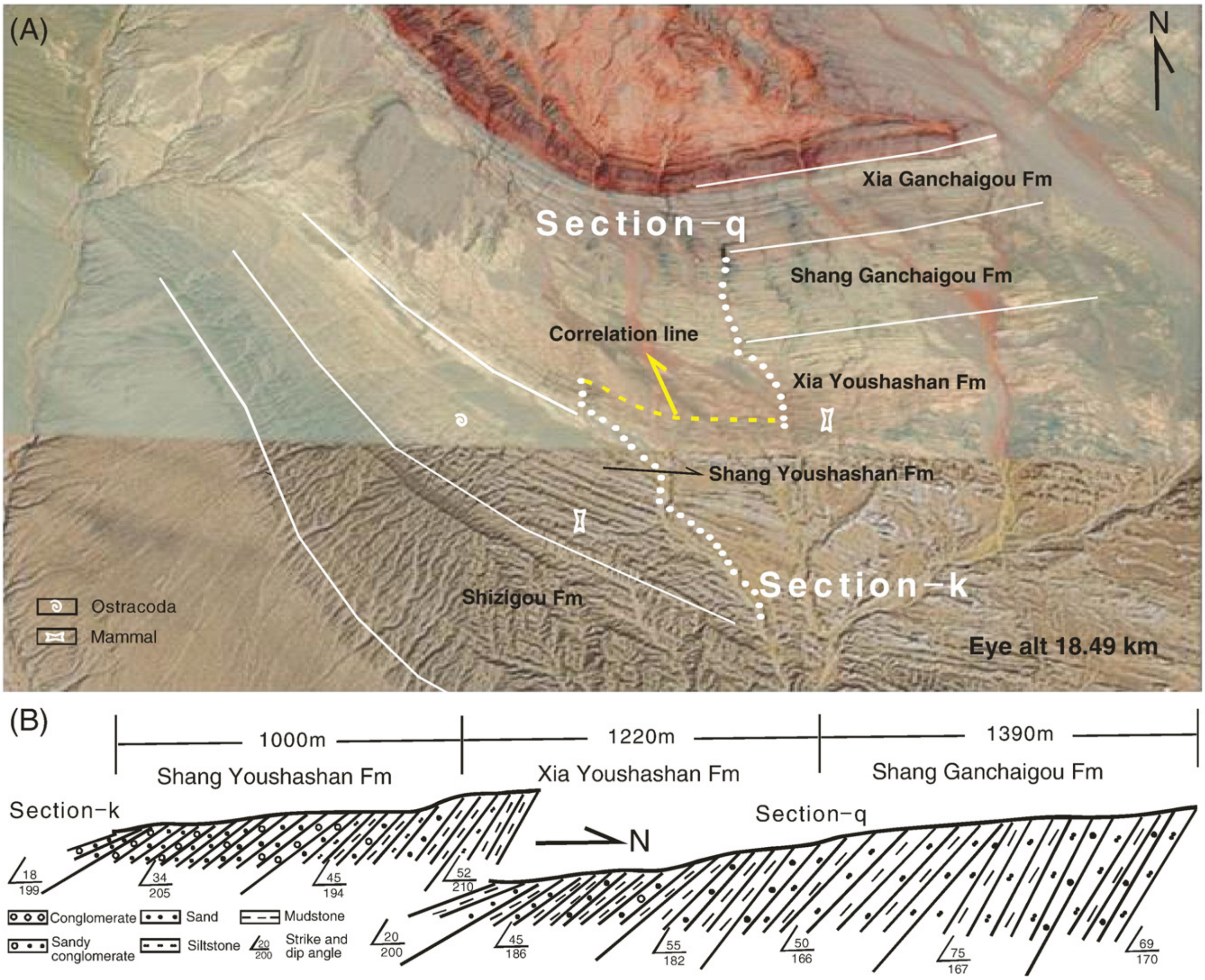

Fig. 3. (A) Google Earth image of the Dahonggou section showing stratigraphy, sampling sections and the approximate locations of ostracoda and mammal fossils (Qinghai BGMR, 1984). Note that the lower part of section-k and the upper part of section-q overlap lithologically with a thickness of ~100 m. (B) Composite cross section of the sedimentary succession exposed in the Dahonggou section. Note that the stratigraphy of section-q exhibit a steeper dip than that of section-k.

and orthogonal diagrams (Zijderveld, 1967). The characteristic remanent directions were determined by principal component analysis (Kirschvink, 1980) and interval-mean directions were calculated with Fisher statistics (Fisher, 1953).

4. Paleomagnetic results and analyses

Progressive thermal demagnetization revealed two magnetic components following removal of a soft viscous overprint by temperature step 150 °C (Fig. 4A–J). The low-temperature magnetic component was usually removed below 400 °C (Fig. 4A, C–J) and thought to be of post-folding origin and may be a recent overprint (Huang et al., 2004). The high temperature was generally isolated between 300 (Fig. 4A, B, D, E) or 350 °C (Fig. 4G, H) and 680 °C, or between 500 °C (Fig. 4C, F, I) and 680 °C. From the unblocking temperatures of ~575 °C (Fig. 4F–H) and ~680 °C (Fig. 4A–J), we can simply infer that magnetite and hematite are the characteristic remnant magnetic (ChRM) carriers. Specifically, the major ChRM carriers are hematite (Fig. 4A, B), and magnetite (Fig. 4F–H) and hematite (Fig. 4C–J) in coarse-grained and relatively fine-grained samples, respectively. As far as all samples are concerned, hematite is the dominant ChRM carrier.

The ChRM direction was determined by at least three, typically five to seven points in the demagnetization trajectory. By principal component analysis, magnetic directions of 926 (out of 1643) samples are interpreted as having been acquired during times of stable polarity. 219 samples, whose directions scatter outside of 40° of the mean direction, are interpreted to have recorded transitional or excursional geomagnetic fields (Gilder et al., 2001; Huang et al., 2006). The remaining ones are discarded for unstable ChRM directions or because the maximum angular deviation (MAD) is $>15°$.

Of all the 1145 (926 plus 219) samples which are used to establish magnetostratigraphy, 640 samples are of normal polarity and 505 samples are of reverse polarity. The mean normal and reverse polarity directions are $D=352.1°$, $I=40°$, $K=8.8$, $\alpha_{95}=2.1$ and $D=174.9°$, $I=-32.3°$, $K=8.7$, $\alpha_{95}=2.3$ after tilt correction respectively. The reversal test is negative at the 95% confidence level with an angular separation of 8°, which is more than the critical angle of 3° (McFadden and McElhinny, 1990) (Fig. 5). The failure is considered to be due to an unremoved overprint (McElhinny et al., 1996; Quidelleur and Courtillot, 1996; Gilder et al., 2001) and further interpreted to be on account of the folding geometry and the present magnetic field direction that steepen the normal polarity direction and shallow the reverse polarity direction (Gilder et al., 2001).

The gradual steepening (from ~15° to ~80°) of structural dip in the Dahonggou section allows us to apply with a fold test. We select sites 3 and 5 (derived from grouping of stratigraphy) from the top and base of section-q respectively, each site with an average thickness of ~50–80 m (Table 1). The fold test, which is based on the eight sites, is

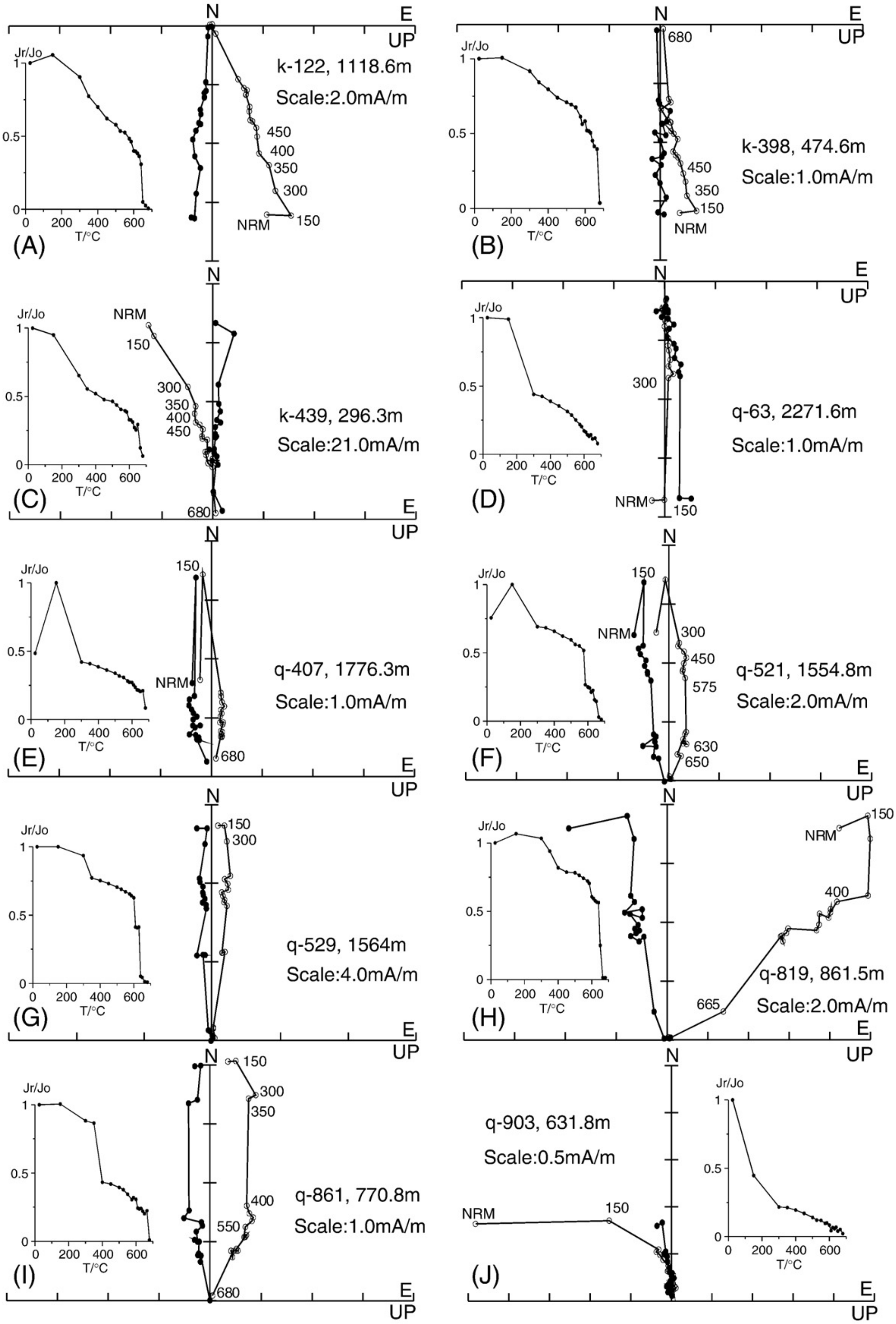

Fig. 4. Orthogonal demagnetization diagrams of representative specimens from the Dahonggou section. Solid (open) symbols refer to the projection on the horizontal (vertical) plane in geographic coordinates. The numbers refer to the temperature in °C.

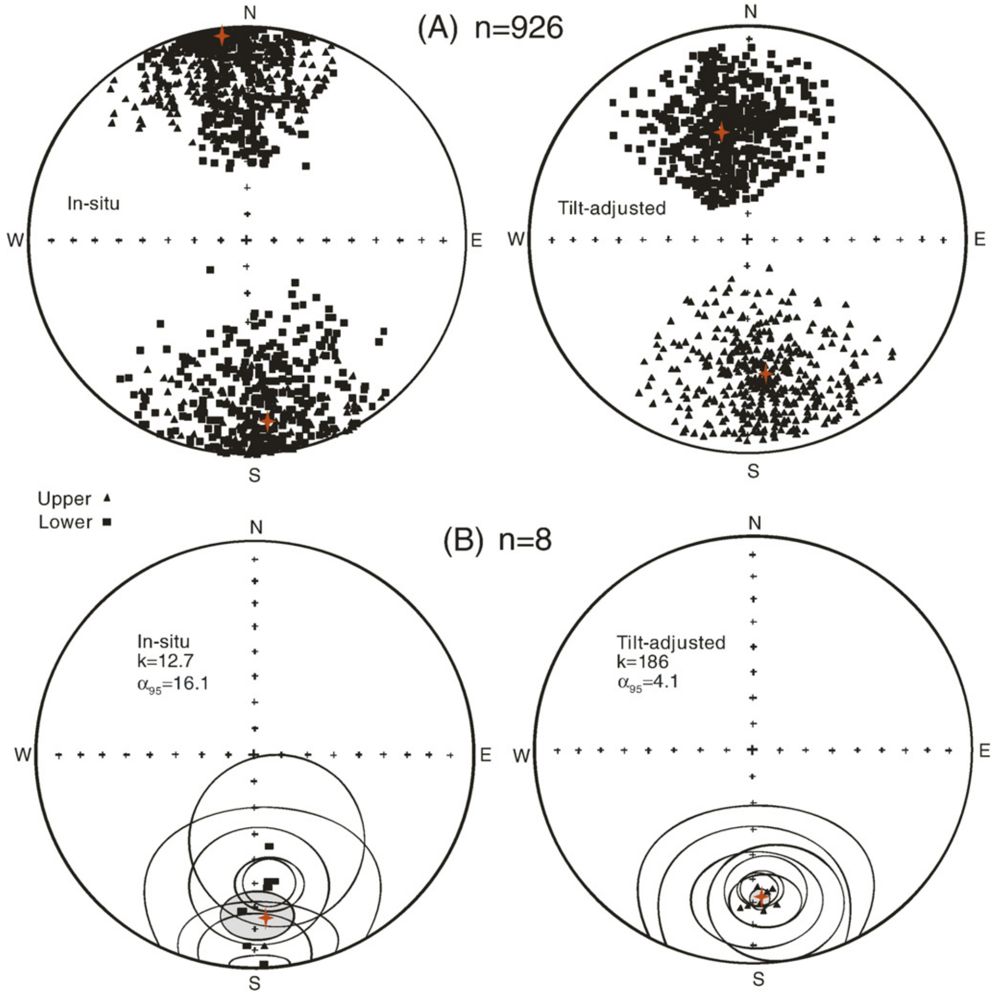

Fig. 5. Equal area projections of: (A) 926 ChRM directions; (B) 8 site-mean directions (Table 1) of ChRM from section-q before and after tilt adjustment. The triangle (rectangle) symbols represent upward (downward) inclinations and the red symbols indicate mean directions.

clearly positive, because the precision parameter increases 14.6 times from in situ to tilt-corrected coordinates (Fig. 5), which indicates that the ChRM direction was acquired at, or close to, the time of rock formation.

5. Magnetostratigraphy

A magnetostratigraphic sequence (Fig. 6) is established based on samples that reflect stable ChRM directions, and a total of 39 pairs of normal and reversed polarity zones is identified in the composite section. As discussed above, Ostracoda and Mammal fossils give an age constraint of late Miocene for the upper part of Shang Youshashan formation, 12 Ma to late Miocene for the middle part of Shang Youshashan formation, and Mid-Miocene for the upper part of Xia Youshashan formation. Based on these age constraints, we can readily correlate the magnetic polarity with the geomagnetic polarity timescale (GPTS) (Lourens et al, 2004) (Fig. 6). We give particular weight to matching long normal polarity zones N5 and N21 with

Table 1
Summary of the interval-mean directions of ChRM from the section-q.

Site ID	Depth (m)	Strike/dip	n/no	N/R	Dg	Ig	Ds	Is	Kg/Ks	α_{95}g/α_{95}s
1	0–45.9	195/33	30/31	3/27	176.8	−11.8	174.5	−34.2	3.4/3.5	17/16.6
2	66.6–115.4	170/38	19/19	0/19	177.1	1.3	178.5	−36.3	20.9/22.2	7.5/7.3
3	120.8–195.8	188/44	10/12	0/10	181.7	11.8	182.2	−29.3	6.3/6.3	20.9/20.9
4	1891.6–1969.4	182/60	19/21	5/14	184.5	28.6	184.5	−26.9	1.6/1.6	42.4/42
5	1987.3–2055.8	180/80	13/15	2/11	172	54.5	175.8	−26.6	2.4/2.4	34.4/34.8
6	2057.2–2121.5	180/77	18/21	0/18	171.6	40	172.1	−36.8	9.5/9.7	11.8/11.7
7	2122.9–2188.7	192/75	14/15	0/14	175	38.2	175.6	−29.5	11.5/10.2	12.2/13.1
8	2311.7–2386.4	168/64	12/15	1/11	172.6	39.1	170.4	−27.4	3.6/3.6	26.9/26.7
Mean			8/8	0/8	176.9	25.5	176.7	−31	12.7/186	16.1/4.1

Abbreviations are: Site ID, site identification; Strike/dip, strike azimuth and dip of bed which are given by average values; n/no, numbers of samples or sites used to calculation/yielded well-defined ChRM or demagnetized; N/R, samples or sites show normal/reversed polarity; Dg and Ig, *K*, α_{95} (Ds and Is, *K*, α_{95}), declination and inclination of direction, precision parameter, 95% confidence limit of Fisher statistics in situ (after tilt adjustment).

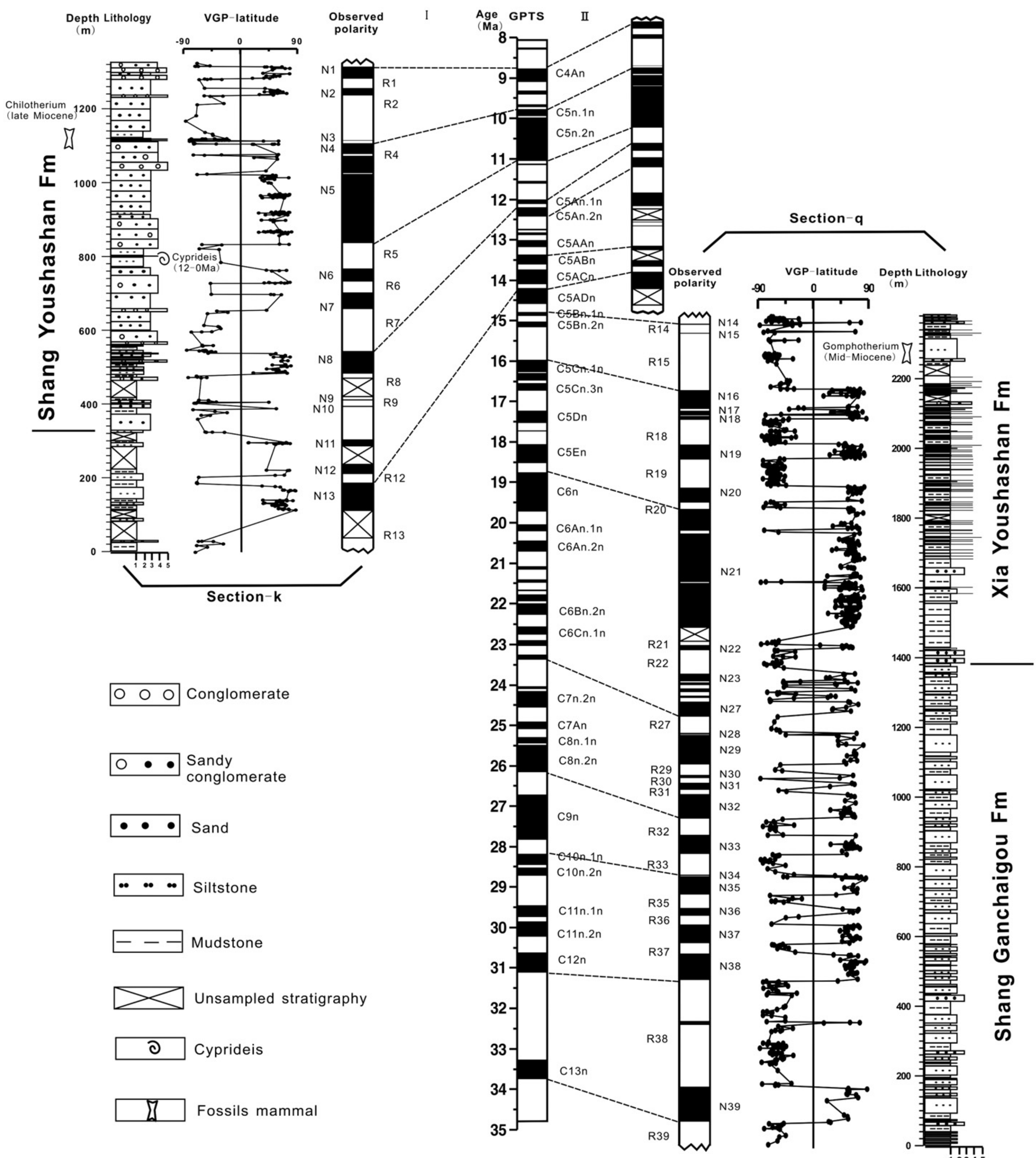

Fig. 6. Lithology and magnetostratigraphic results from the Dahonggou section with VGP latitude against stratigraphic level and correlation with the GPTS of Lourens et al. (2004). Two correlations (I and II) are provided for polarity zones of R5 to N12 and correlationIis preferred. The horizontal scales in the stratigraphy column are 1 — mudstone; 2 — siltstone; 3 — sandstone; 4 — sandy conglomerate; 5 — conglomerate.

C5n.2n and C6n, long reversed polarity zones R15 and R38 with C5Br and C12r, respectively. Those observed polarity zones can be well correlated with chrons C4An to C13r of the GPTS except for polarity zones of R5 to N12 as a result of poor sampling resolution in section-k and the exceptionally long normal polarity zone N21 in section-q. Two correlations (I and II) are provided for the polarity zones of R5 to N12 and correlation I is accepted because in the case of correlation I, polarity zones of R5 to R7 with a relatively coarse grain size can obtain a consistent sedimentation rate with the upper part of section-k, and polarity zones of N8 to N12 with a relatively fine grain size can possess a consistent sedimentation rate with section-q. In the field, the stratigraphy of section-k can be divided into two distinct lithofacies as Figs. 6 and 7 show and is free of any big unconformity or discontinuity. In addition, the steady variation of magnetic susceptibility for both lithofacies does not advocate any reorganization of sediment source related to climate change or tectonic deformation. Based on those observations, we agree that the sedimentary rock with a similar grain size should possess a consistent sedimentary rate for the Dahonggou section. As for the exceptionally long normal polarity zone N21, similar situations at ~20 Ma were likewise encountered in Tarim Basin and Xining Basin (Huang et al., 2006; Guoqiao Xiao, personal communication) and we did not recognize

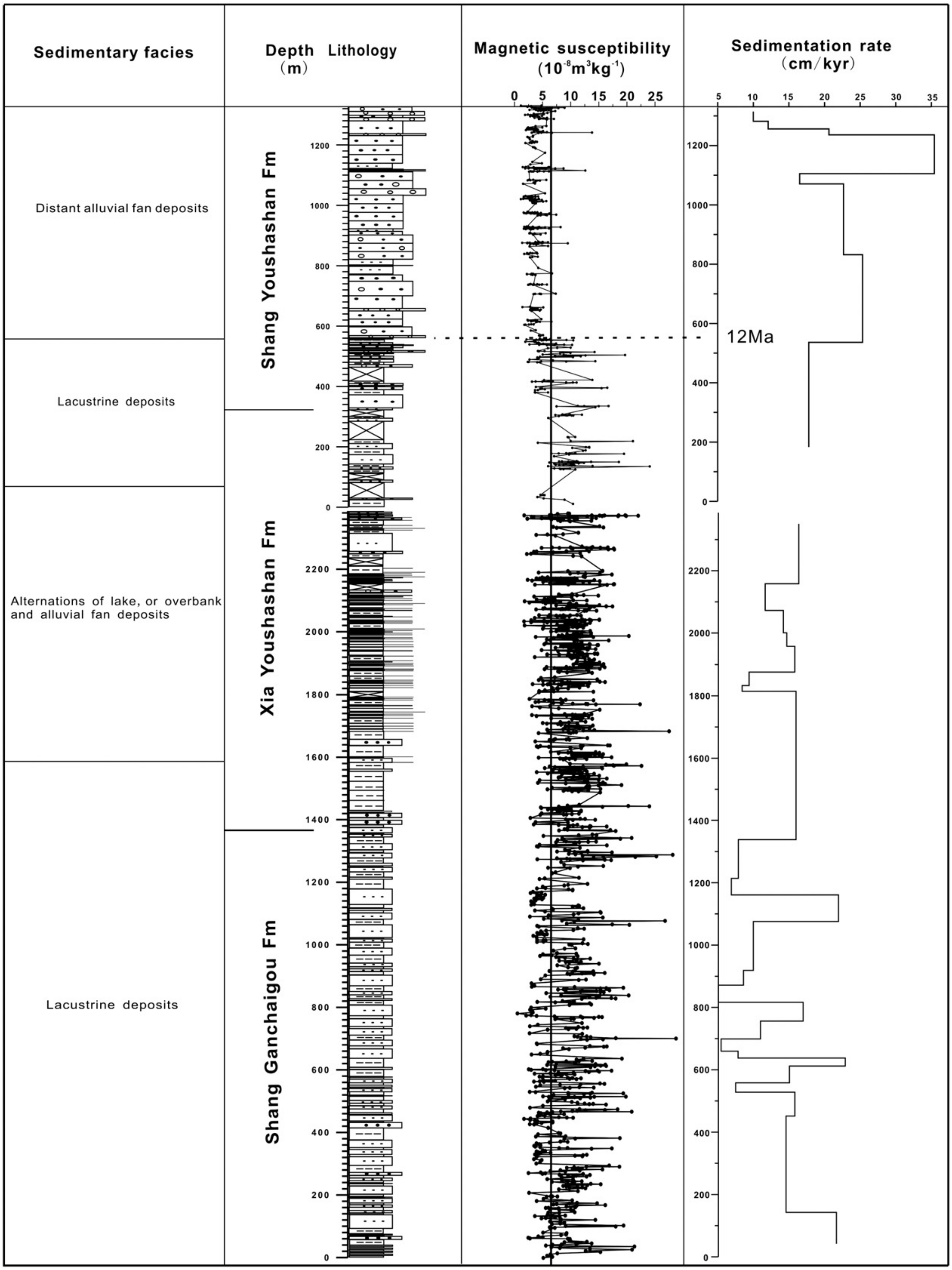

Fig. 7. Lithology, sedimentary facies, magnetic susceptibility and sedimentation rate of the Dahonggou section. The lithology legends are the same as in Fig. 6. The sedimentation rates are calculated based on the stratigraphic depths and magnetochrons from the magnetostratigraphic correlation in Fig. 6.

any stratigraphic abnormality in the field. In light of the occurrences of conglomerate deposits at ~21–20 Ma, we relate it to the rejuvenation of nearby fold and thrust belts.

The following conclusions are readily drawn on the basis of correlation I, the Dahonggou section spans 25.5 Ma from ~34 to ~8.5 Ma, the Shang Youshashan formation spans ~4.5 Ma ranging through ~13 to ~8.5 Ma, the Xia Youshashan formation spans ~8 Ma from ~22–20 Ma to ~13 Ma, the Shang Ganchaigou formation spans ~13 Ma from ~34 to ~22–20 Ma.

6. Discussion

6.1. The transition of sediment source inferred from the variation of magnetic susceptibility of bulk samples (K) and a revised conceptual model of K variation as a response of tectonic deformation

The magnetic susceptibility of bulk samples (K) has been widely used in tracking changes in potential sediment sources (Gilder et al., 2001; Sun et al., 2005a; Charreau et al., 2005, 2006; Huang et al., 2006). The K values of the Dahonggou section (Fig. 7) range from 1 to $25\times10^{-8}\,m^3\,kg^{-1}$, suggesting the dominant contribution of hematite in magnetic susceptibility variations (Tarling and Hrouda, 1993; Huang et al., 2006) in the sediments of the Dahonggou section.

The K variations along the section exhibit an abrupt shift at about 12 Ma (Fig. 7). This K value drop can be correlated well with the transition of sedimentary facies and acceleration of sedimentation rate at a depth of ~564 m in the section-k (Fig. 7). At this boundary, the sedimentary cyclicity of mud and siltstone, or sandstone, or conglomerate disappears and is replaced by massive sandstone, siltstone and conglomerate. Moreover, the average sedimentation rate goes up abruptly to ~22.6 cm/kyr (Fig. 7), though greatly lower than ~39 cm/kyr at 14.7 Ma in the Huaitoutala section (Fang et al., 2007), ~130 km east of the Dahonggou section (Figs. 1 and 2). Thus, those significant transitions at 12 Ma would signal a radical departure in potential sediment sources.

Previous studies have revealed that there is an obvious K pulse for the sediments in the foreland basin when the surrounding mountains begin to uplift rapidly (Gilder et al., 2001; Sun et al., 2005a; Charreau et al., 2006; Huang et al., 2006). Sun et al. (2005a) have proposed a conceptual model to explain the increase of K as a response to tectonic uplift. They pointed out that those coarse clastic particles with both magnetite and hematite were quickly transported to the foreland basin during active tectonic periods, however, during periods of stable tectonics, source materials had undergone prolonged in situ chemical weathering and most of the magnetite had oxidized to hematite (Sun et al., 2005a).

On the contrary, our study indicates the K decreases significantly as a response to the tectonic deformation and as discussed above, hematite is the major magnetic-bearing mineral for the Dahonggou section. By simple comparison, the distance between the mountain front and depositional basin may hold the key for the difference. Unlike other foreland basins, the Dahonggou section is very close (40 km) to the Quaternary depocenter (the Dabsan depression) of the Qaidam Basin (Fig. 2A) and clastic particles have traveled further before deposition.

Based on the conceptual model by Sun et al. (2005a), we developed a revised conceptual model (Fig. 8) to interpret the different responses of the K values of the basin sediments to the source area uplift. In the model (Fig. 8), site A mark the situation described by Sun et al. (2005a) and is closer to the mountain front than site B. For site B, during tectonically quiet period the bedrock enriched in magnetite underwent

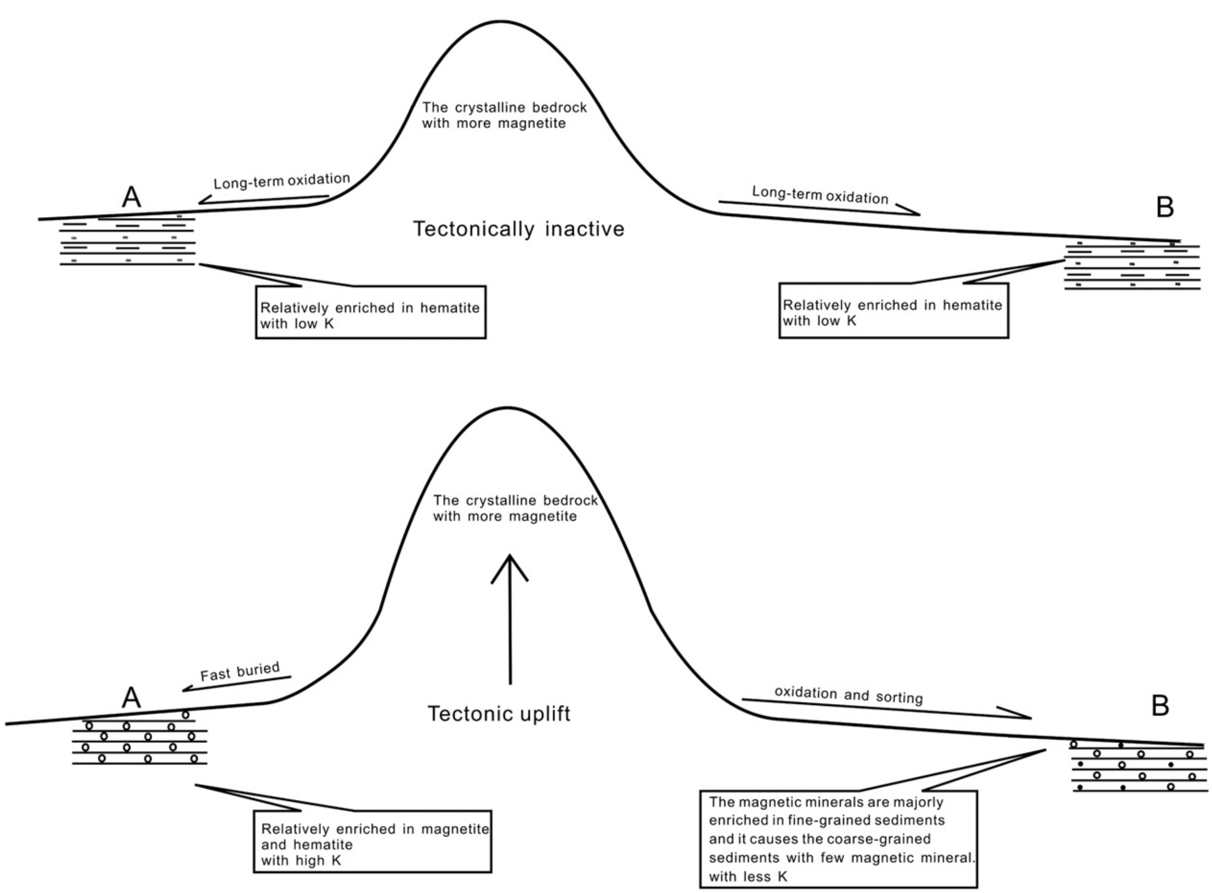

Fig. 8. The conceptual model used to explain the discrepancy of K variations in response to tectonic uplift in different sites. Site A is closer to the mountain front than site B.

long-term weathering, with magnetite being oxidized to hematite, before forming sediments rich in hematite. However, when tectonically active, in the course of transport, weathering and sorting, magnetite was oxidized to hematite and the magnetic mineral was diluted by coarse-grained sediments (mainly quartz and other clasts), which both caused coarse-grained sediments in the deposition zone (site B) to bear few magnetic mineral. The model is well supported by the correlation analysis between *K* and the grain size of 289 samples equidistantly selected from the entire section, which suggested *K* displays a relatively strong positive correlation with fine-grained size-fraction (<10 μm), and a relatively strong negative correlation with coarse-grained size-fraction (>70 μm) (Fig. 9).

6.2. Implications for the tectonic history of the Qilian Shan and Altyn Tagh Fault

The variations in lithofacies, sedimentation rates and *K* values along the Dahonggou section imply that the Qilian Shan has been tectonically inactive at 30 Ma. This is inconsistent with the suggestion of Sun et al. (2005b). Based on the variations of lithofacies and sedimentation rates in the Hongsanhan section (Figs. 1 and 2A), nearby the Altyn Tagh Fault, Sun et al. (2005b) concluded that there is a rapid deformation event in the mountain ranges (northern Qaidam and east Kunlun) surrounding the Qaidam Basin at around 30 Ma, which may reflect the early growth of the Tibetan Plateau due to the India–Asia collision. However, caution is necessary when interpreting the tectonic history of mountains based on sedimentary record from a single section (Métivier and Gaudemer, 1997; Métivier et al., 1999), and we speculate that variations in lithofacies and sedimentation rates in the Hongsanhan section at about 30 Ma (Sun et al., 2005b) may be a direct response to large magnitude strike-slip faulting on the Altyn Tagh Fault initiated in the Oligocene (Hanson, 1999; Rumelhart, 1999; Yue et al., 2003). The asynchronous sedimentary shifts between the Dahonggou section and Hongsanhan section may indicate that the southern Qilian Shan did not respond to this Oligocene–earliest Miocene rapid slip on the Altyn Tagh Fault (Ritts et al., 2008).

Those major transitions in lithofacies, sedimentation rate and *K* at ~12 Ma observed in the Dahonggou section seem mainly due to tectonic uplift rather than climate change. Supporting evidence for a tectonic interpretation includes: (1) The pollen sequence of Qaidam Basin and Tian Shan ranges both indicate the Miocene was characterized by the predominance of a relatively less dry and stable climate (Wang et al., 1999; Sun et al., 2008). (2) The duration and consistency of the susceptibility signature imply that this is a tectonic signature rather than the result of climate-induced pedogenesis (Gilder et al., 2001; Sun et al., 2005a; Huang et al., 2006). Although the rapid uplift of the Qilian Shan is a preferred candidate for interpretation, the climatic role cannot be excluded. For example, recently Jiang et al (2008) identified a cooling-driven event at 12–11 Ma from multiproxy records of a long fluviolacustrine sequence at Guyuan, Ningxia, located to the east of the arid region of northwestern China. This finding thus implies that global cooling and the development of the East Antarctic Ice Sheet since about 14 Ma would have imprinted on semiarid and even arid regions of China. Dettman et al. (2003) also document an increase in aridity on the northeastern margin of the Tibetan Plateau by the shift of $\delta^{18}O$ values of lacustrine carbonates in the Linxia basin between ca. 13 and 12 Ma. For the Dahonggou section, global cooling would have induced the development of glacial and periglacial erosion in surrounding mountains, possibly causing the coarse-grained sedimentation and relatively high sedimentation rate.

Those major transitions at ~12 Ma in the Dahonggou section can be attributed to the tectonic uplift of the southern Qilian Shan, rather than local deformation because the counter-intuitive *K* variations do not justify a proximal source area and facies analyses indicate a distal alluvial fan deposits after 12 Ma (Fig. 7).

The 12 Ma tectonic event observed in the Dahonggou section exhibits discrepancy in timing with the tectonic uplift event (~14.7 Ma) observed in the Huaitoutala section (Fang et al., 2007) (Figs. 1 and 2). Two possibilities may be used to explain this difference. First, the Dahonggou and the Huaitoutala sections may record different thrust events. Secondly, due to the different distances from the deformation source areas, the Dahonggou and the Huaitoutala sections may respond with a different lag time to the same tectonic uplift event. We cannot discriminate which one is more probable.

Nevertheless, the observed 12 Ma transition in the Dahonggou section has its counterpart. A paleomagnetic study (Wang et al., 2003) from the Xishuigou section along the Altyn Tagh Fault (Fig. 1) displays an important event at about 12 Ma, with sediments gradually coarsening from fine-grained particles to boulder conglomerates, which broadly exist along much of the Qilian range front (Wang et al., 2003; Ritts et al., 2008; Bovet et al., 2009). Other paleomagnetic studies in northern Tibet Plateau likewise identify tectonic uplift events at 14–11 Ma (Sun et al., 2005a; Charreau et al., 2005, 2006). At the margin of the Tibet Plateau, such as the Tarim basin, the Sichuan basin, the Linxia basin, northern Qilian Shan, etc, sufficient evidence from various kinds

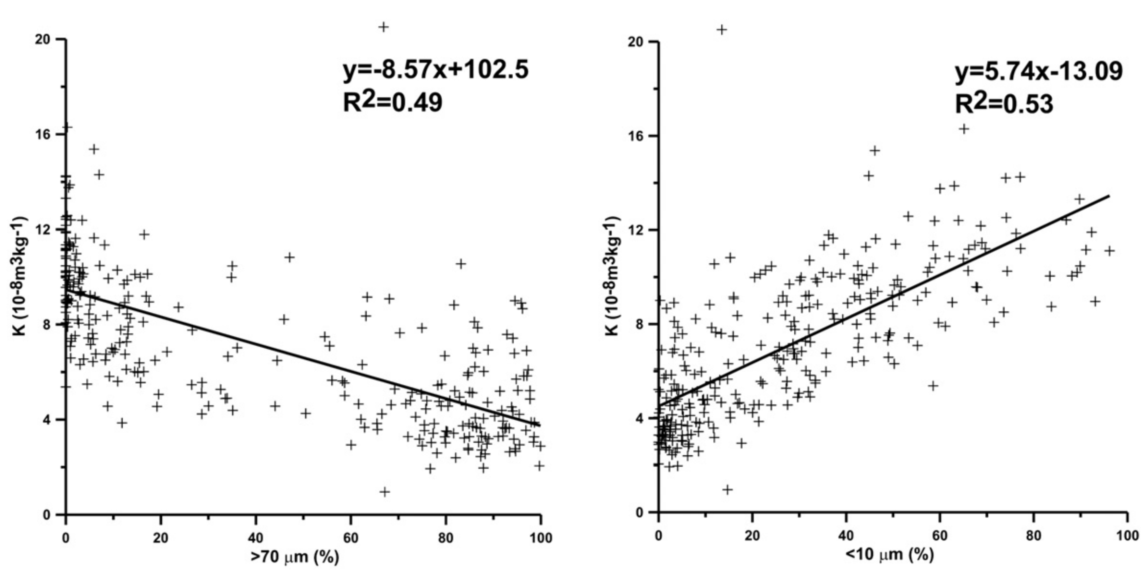

Fig. 9. The correlation analyses diagram between K and grain size of 289 samples equidistantly selected from the entire section.

of thermochronological data, Nd isotope, and paleomagnetic age of river terrace collectively suggests that the Tibet Plateau began to uplift and grow outward significantly at 14–12 Ma (Sobel and Dumitru, 1997; George et al., 2001; Kirby et al., 2002; Zheng et al., 2003; Lu et al., 2004; Clark et al., 2005; Garzione et al., 2005; Bovet et al., 2009). Those may indicate that the observed sedimentary change at about 12 Ma in the Dahonggou section was due to a regional rather than a local uplift event. Thus, speculatively, sedimentary changes proximal to the Altyn Tagh Fault and the Qilian Shan at ~12 Ma may have been a northern plateau-wide event resulted from the India–Asia collision.

7. Conclusion

The detailed magnetostratigraphic study of the Dahonggou section in the Qaidam Basin shows that the composite section spans from ~34 to ~8.5 Ma and the ages of Shang Ganchaigou, Xia Youshashan and Shang Youshashan formations are from > 34 to 22–20 Ma, 22–20 to ~13 Ma and ~13 to < 8.5 Ma, respectively. Sedimentary records suggest that the southern Qilian Shan was tectonically inactive at 30 Ma. It is observed that some major transitions in lithofacies, sedimentation rate, and *K* occurred at about 12 Ma in the Dahonggou section. Those transitions are synchronous with a sedimentary change (12 Ma) at the Xishuigou section along the Altyn Tagh Fault, perhaps indicating that they resulted from a regional rather than a local uplift event. Other evidences further suggest that the ~12 Ma event may be an uplift and outward growth of the northern Tibet Plateau related to the India–Asia collision. In addition, the counter-intuitive *K* variation is interpreted to be due to long-distanced oxidation and sorting, which cause not only that magnetite was oxidated to hematite, but also that magnetic minerals are diluted by quartz and other clasts in the coarse-grained sediments.

Acknowledgment

This study is supported by the Innovation Project of Chinese Academy of Sciences (KZCX2-YW-130, KZCX2-YW-Q05, and KZCX2-SW-133) and NSF of China (grant 40672117). We thank Professor Donghuai Sun for his laboratory support, and Carmala N. Garzione and Brian Horton for their critical and constructive suggestions, which greatly improve the early version of the manuscript. We especially thank Carmala N. Garzione for her kind help with the English improvement. Detailed and thorough reviews by Douglas W. Burbank and Bradley D. Ritts profoundly improved this manuscript. Discussions with Zhiyu Yi, Zihua Tang and Guoqiao Xiao were helpful and appreciated.

References

Bovet, PM., Ritts, B.D., Gehrels, G.G., Abbink, O.A., Darby, B.J., Hourigan, J., 2009. Evidence of Miocene crustal shortening in the North Qilian Shan from Cenozoic stratigraphy of the Western Hexi Corridor. Am. J. Sci. 309, 290–329.

Charreau, J., Chen, Y., Gilder, S., et al., 2005. Magnetostratigraphy and rock magnetism of the Neogene Kuitun He section (northwest China): implications for Late Cenozoic uplift of the Tian Shan mountains. Earth Planet. Sci. Lett. 230, 177–192.

Charreau, J., Gilder, S., Chen, Y., Dominguez, S., Avouac, J.P., Sevket, S., Jolivet, M., Li, Y., Wang, W., 2006. Magnetostratigraphy of the Yaha section, Tarim Basin (China): 11 Ma acceleration in erosion and uplift of the Tian Shan mountains. Geology 34, 181–184.

Chen, W.P., Chen, C.Y., Nábelek, J.L., 1999. Present-day deformation of the Qaidam basin with implications for intra-continental tectonics. Tectonophysics 305, 165–181.

Chen, J., Burbank, D.W., Scharer, K.M., Sobel, E., Yin, J.H., Rubin, C., Zhao, R.B., 2002. Magnetochronology of the Upper Cenozoic strata in the southwestern Chinese Tian Shan: rates of Pleistocene folding and thrusting. Earth Planet. Sci. Lett. 195, 113–130.

Clark, M.K., House, M.A., Royden, L.H., Whipple, K.X., Burchfiel, B.C., Zhang, X., Tang, W., 2005. Late Cenozoic uplift of southeastern Tibet. Geology 33, 525–528.

Dai, J.S., Ye, X.S., Tang, L.J., Jin, Z.J., Shao, W.B., Hu, Y., Zhang, B.S., 2003. Tectonic units and oil–gas potential of the Qaidam Basin. Chin. J. Geol. 38, 291–296.

Dai, S., Fang, X.M., Song, C.H., Gao, J.P., Gao, D.L., Li, J.J., 2005. Early tectonic uplift of the northern Tibetan Plateau. Chin. Sci. Bull. 50, 1642–1652.

Dai, S., Fang, X.M., Dupont-Nivet, G., Song, C.H., Gao, J.P., Krijgsman, W., Langereis, C., Zhang, W.L., 2006. High-resolution magnetostratigraphy of Cenozoic sediments in Xining Basin and its implication on tectonic deformation and uplift of the northeastern Tibetan Plateau. J. Geophys. Res. 111.

Deng, T., 2004. Establishment of the middle Miocene Hujialiang Formation in the Linxia Basin of Gansu and its features. J. Stratigr. 28, 307–312.

Deng, T., 2005. Character, age and ecology of the Hezheng Biota from Northwestern China. Acta Geol. Sin. 79, 739–750.

Deng, T., Wang, X.M., Ni, X.J., Liu, L.P., 2004. Sequence of the Cenozoic mammalian faunas of the Linxia Basin in Gansu, China. Acta Geol. Sin. 78, 8–14.

Deng, T., Hou, S.K., Wang, H.J., 2007. The Tunggurian stage of the continental Miocene in China. Acta Geol. Sin. 81, 709–721.

Dettman, D.L., Fang, X.M., Garzione, C.N., Li, J.J., 2003. Uplift-driven climate change at 12 Ma: a long $\delta^{18}O$ record from the NE margin of the Tibetan plateau. Earth and Planetary Science Letters 214, 267–277.

Di, H.S., Wang, S.G., 1991. The study of the evolution of the Mesozoic and Cenozoic structures in the northeast margin of Qaidam Basin. J. China Univ. Geosci. 16, 533–539.

England, P.C., Houseman, G.A., 1989. Extension during continental convergence with application to the Tibetan plateau. J. Geophys. Res. 94, 17561–17579.

Fang, X.M., Garzione, C., VanderVoo, R., Li, J.J., Fan, M.J., 2003. A flexural subsidence by 29 Ma on the NE edge of Tibet from the magnetostratigraphy of Linxia Basin. China. Earth Planet. Sci. Lett. 210, 545–560.

Fang, X.M., Yan, M.D., VanderVoo, R., Rea, D.K., Song, C.H., Pares, J.M., Nile, J.S., Gao, J.P., Dai, S., 2005a. Late Cenozoic deformation and uplift of the NE Tibetan Plateau: evidence from high-resolution magnetostratigraphy of the Guide Basin, Qinghai Province, China. Geol. Soc. Amer. Bull. 117, 1208–1225.

Fang, X.M., Zhao, Z.J., Li, J.J., Yan, M.D., Pan, B.T., Song, C.H., Dai, S., 2005b. Magnetostratigraphy of the late Cenozoic Laojunmiao anticline in the northern Qilian Mountains and its implications for the northern Tibetan Plateau uplift. Sci. China Ser. D Earth Sci. 48, 1040–1051.

Fang, X.M., Zhang, W.L., Meng, Q.Q., et al., 2007. High-resolution magnetostratigraphy of the Neogene Huaitoutala section in the eastern Qaidam Basin on the NE Tibetan Plateau, Qinghai Province, China and its implication on tectonic uplift of the NE Tibetan Plateau. Earth Planet. Sci. Lett. 258, 293–306.

Fisher, R.A., 1953. Dispersion on a sphere. Proc. R. Soc. Lond. A Math. Phys. Sci. 217, 295–305.

Garzione, C.N., Ikari, M.J., Basu, A.R., 2005. Source of Oligocene to Pliocene sedimentary rocks in the Linxia Basin in northeastern Tibet from Nd isotopes: implications for tectonic forcing of climate. Geol. Soc. Amer. Bull. 117, 1156–1166.

George, A.D., Marshallsea, S.J., Wyrwoll, K.H., Chen, J., Lu, Y.C., 2001. Miocene cooling in the northern Qilian Shan, northeastern margin of the Tibetan plateau, revealed by apatite fission-track and vitrinite-reflectance analysis. Geology 29, 939–942.

Gilder, S.A., Chen, Y., Sevket, S., 2001. Oligo-Miocene magnetostratigraphy and rock magnetism of the Xishuigou section, Subei (Gansu Province, western China) and implications for shallow inclinations in central Asia. J. Geophys. Res. 106, 30505–30522.

Hanson, 1999. Organic geochemistry and petroleum geology, tectonics and basin analysis of the southern Tarim and northern Qaidam basins, northwest China. Ph.D. dissertation. Stanford University, Stanford, pp. 388.

Harrison, T.M., Copeland, P., Kidd, W.S.F., Yin, A., 1992. Raising Tibet. Science 255, 1663–1670.

Harrison, T.M., Yin, A., Ryerson, F.J., 1998. Orographic evolution of the Himalaya and Tibetan plateau. In: Crowley, T.J., Burke, K.C (Eds.), Tectonic Boundary Conditions for Climatic Reconstructions (1998). Oxford Monographs on Geology and Geophysics, vol. 39. Oxford University Press, New York, pp. 40–42.

Heermance, R.V., Chen, J., Burbank, D.W., Wang, C.S., 2007. Chronology and tectonic controls of Late Tertiary deposition in the southwestern Tian Shan foreland, NW China. Basin Res. 19, 599–632.

Heermance, R.V., Chen, J., Burbank, D.W., Miao, J.J., 2008. Temporal constraints and pulsed Late Cenozoic deformation during the structural disruption of the active Kashi foreland, northwest China. Tectonics 27, TC6012–TC6039.

Huang, X.Z., Shao, H.S., 1993. Sedimentary characteristics and types of hydrocarbon source rocks in the Tertiary semiarid to arid lake basins of northwest China. Palaeogeogr. Palaeoclimatol. Palaeoecol. 103, 33–43.

Huang, H.C., Huang, Q.H., Ma, S., 1996. Geology of Qaidam Basin and Its Petroleum Prediction. Geological Publishing House, Beijing, p. 257.

Huang, B.C., Wang, Y.C., Zhu, R.X., 2004. New paleomagnetic and magnetic fabric results for Early Cretaceous rocks from the Turpan intramontane basin, east Tianshan, northwest China. Sci China Ser. D Earth Sci. 47, 540–550.

Huang, B.C., Piper, J.D.A., Peng, S.T., Liu, T., Li, Z., Wang, Q.C., Zhu, R.X., 2006. Magnetostratigraphic study of the Kuche Depression, Tarim Basin, and Cenozoic uplift of the Tian Shan Range, Western China. Earth Planet. Sci. Lett. 251, 346–364.

Jiang, H.C., Ji, J.L., Gao, L., Tang, Z.H., Ding, Z.L., 2008. Cooling-driven climate change at 12–11 Ma: multiproxy records from a long fluviolacustrine sequence at Guyuan, Ningxia, China. Palaeogeogr. Palaeoclimatol. Palaeoecol. 265, 148–158.

Kirby, E., Reiners, P.W., Krol, M.A., Whipple, K.X., Hodges, K.V., Farley, K.A., Tang, W., Chen, Z., 2002. Late Cenozoic evolution of the eastern margin of the Tibetan Plateau: Inferences from $^{40}Ar/^{39}Ar$ and (U–Th)/He thermochronology. Tectonics 21, 1–20.

Kirschvink, J.L., 1980. The least-squares line and plane and the analysis of paleomagnetic data. Geophys. J. R. Astron. Soc. 62, 699–712.

Li, J.J., Fang, X.M., VanderVoo, R., et al., 1997. Late Cenozoic magnetostratigraphy (11–0 Ma) of the Dong Shan ding and Wang Jia Shan sections in the Long Zhong Basin, western China. Geol. Mijnb. 76, 121–134.

Liu, Z.C., Wang, J., Wang, Y.J., et al., 1996. On lower Tertiary chronostratigraphy and climatostratigraphy of Mangyai Depression in western Qaidam Basin. J. Stratigr. 20, 104–113.

Liu, Z.F., Zhao, X.X., Wang, C.S., Liu, S., Yi, H.S., 2003. Magnetostratigraphy of Tertiary sediments from the Hoh Xil Basin: implications for the Cenozoic tectonic history of the Tibetan Plateau. Geophys. J. Int. 154, 233–252.

Liu, Z.H., Wang, C.B., Yang, J.G., 2005. Cenozoic structural characters and deformation rules in northern Qaidam basin. Chin. J. Geol. 40, 404–414.

Lourens, L.J., Hilgen, F.J., Laskar, J., Shackleton, N.J., Wilson, D., 2004. The Neogene period. In: Gradstein, F.M., Ogg, J.G., Smith, A.G. (Eds.), A Geologic Time Scale. Cambridge University Press, Cambridge, UK, pp. 409–440.
Lu, H.Y., An, Z.S., Wang, X.Y., et al., 2004. Geomorphologic evidence of phased up lift of the northeastern Qinghai–Tibet Plateau since 14 million years. Sci. China Ser. D 34, 855–864.
McElhinny, M.W., McFadden, P.L., Merrill, R.T., 1996. The time-averaged paleomagnetic field 0–5 Ma. J. Geophys. Res. 101, 25007–25028.
McFadden, P.L., McElhinny, M.W., 1990. Classification of the reversal test in palaeomagnetism. Geophys. J. Int. 103, 725–729.
Meng, Q.R., Hu, J.M., Yang, F.Z., 2001. Timing and magnitude of displacement on the Altyn Tagh fault: constraints from stratigraphic correlation of adjoining Tarim and Qaidam basins, NW China. Terra Nova 13, 86–91.
Métivier, F., Gaudemer, Y., 1997. Mass transfer between eastern Tien Shan and adjacent basins (central Asia): constraints on regional tectonics and topography. Geophys. J. Int. 128, 1–17.
Métivier, F., Gaudemer, Y.P., Tapponnier, B.Meyer, 1998. Northeastward growth of the Tibet Plateau deduced from balanced reconstruction of two depositional areas: the Qaidam and Hexi Corridor basins, China. Tectonics 17, 823–842.
Métivier, F., Gaudemer, Y., Tapponnier, P., Klein, M., 1999. Mass accumulation rates in Asia during the Cenozoic. Geophys. J. Int. 137, 280–318.
Molnar, P., England, P., Martinod, J., 1993. Mantle dynamics, uplift of the Tibetan Plateau, and the Indian monsoon. Rev. Geophys. 31, 357–396.
Pang, X.Q., Li, Y.X., Jiang, Z.X., 2004. Key geological controls on migration and accumulation for hydrocarbons derived from mature source rocks in Qaidam Basin. J. Pet. Sci. Eng. 41, 79–95.
Pares, J.M., VanderVoo, R., Downs, W.R., Yan, M.D., Fang, X.M., 2003. Northeastward growth of the Tibetan Plateau: magnetostratigraphic insights from the Guide basin. J. Geophys. Res. 108, 1–11.
Qinghai BGMR, 1984. Geologic map of the Daqaidam Sheet: Beijing Geological Publishing House, scale 1:200,000.
Quidelleur, X., Courtillot, V., 1996. On low degree spherical harmonic models of paleosecular variation. Phys. Earth Planet. Inter. 95, 55–77.
Rieser, A.B., Neubauerb, F., Liu, Y.J., Ge, X.H., 2005. Sandstone provenance of north-western sectors of the intracontinental Cenozoic Qaidam basin, western China: tectonic vs. climatic control. Sed. Geol. 177, 1–18.
Ritts, B.D., Yue, Y., Graham, S.A., Sobel, E.R., Abbink, O.A., Stockli, D., 2008. From sea level to high elevation in 15 million years: uplift history of the northern Tibetan Plateau margin in the Altun Shan. Am. J. Sci. 308, 657–678.
Rumelhart, P.E., 1999. Cenozoic basin evolution of southern Tarim, northwestern China: implications for the uplift history of the Tibetan Plateau. Ph.D. dissertation. Los Angeles, University of California, pp. 268.
Sobel, E.R., Dumitru, T.A., 1997. Thrusting and exhumation around the margins of the western Tarim basin during the India–Asia collision. J. Geophys. Res 102, 5043–5063.
Song, C.H., Fang, X.M., Li, J.J., Gao, J.P., Fan, M.J., 2001. Tectonic uplift and sedimentary evolution of the Jiuxi Basin in the northern margin of the Tibetan Plateau since 13 Ma BP. Sci. China Ser. D Earth Sci. 44, 92–202 Suppl.
Sun, J.M., Zhang, Z.Q., 2008. Palynological evidence for the Mid-Miocene Climatic Optimum recorded in Cenozoic sediments of the Tian Shan Range, northwestern China. Glob. Planet. Change 64, 53–68.
Sun, J.M., Zhang, Z.Q., 2009. Syntectonic growth strata and implications for late Cenozoic tectonic uplift in the northern Tian Shan, China. Tectonophysics 463, 60–68.
Sun, Z.C., Feng, X., Li, D., Yang, F., Qu, Y., Wang, H., 1999. Cenozoic Ostracoda and palaeoenvironments of the northeastern Tarim Basin, western China. Palaeogeogr. Palaeoclimatol. Palaeoecol. 148, 37–50.
Sun, J.M., Zhu, R.X., Bowler, J., 2004. Timing of the Tian Shan Mountains uplift constrained by magnetostratigraphic analysis of molasses deposits. Earth Planet. Sci. Lett. 219, 239–253.
Sun, J.M., Zhu, R.X., An, Z.S., 2005a. Tectonic uplift in the northern Tibetan Plateau since 13.7 Ma ago inferred from molasses deposits along the Altyn Tagh Fault. Earth Planet. Sci. Lett. 235, 641–653.
Sun, Z.M., Yang, Z.Y., Pei, J.L., et al., 2005b. Magnetostratigraphy of Paleogene sediments from northern Qaidam basin, China: implications for tectonic uplift and block rotation in northern Tibetan plateau. Earth Planet. Sci. Lett. 237, 635–646.
Sun, J.M., Zhang, L.Y., Deng, C.L., Zhu, R.X., 2008. Evidence for enhanced aridity in the Tarim Basin of China since 5.3 Ma. Quat. Sci. Rev. 27, 1012–1023.
Tapponnier, P., Xu, Z., Francoise, R., Bertrand, M., Nicolas, A., Gerard, W., Yang, J., 2001. Oblique stepwise rise and growth of the Tibet Plateau. Science 294, 1671–1677.
Tarling, D.H., Hrouda, F., 1993. The Magnetic Anisotropy of Rocks. Chapman and Hall, London, p. 217.
Wang, Q., Coward, M., 1990. The Chaidam basin (NW China): formation and hydrocarbon potential. J. Pet. Geol. 13, 93–112.
Wang, J., Wang, J.Y., Liu, Z.C., Li, J.Q., Xi, P., 1999. Cenozoic environmental evolution of the Qaidam Basin and its implications for the uplift of the Tibetan Plateau and the drying of central Asia. Palaeogeogr. Palaeoclimatol. Palaeoecol. 152, 37–47.
Wang, X.M., Wang, B.Y., Qiu, Z.X., Xie, G.P., Xie, J.Y., Downs, W., Qiu, Z.D., Deng, T., 2003. Danghe area (western Gansu, China) biostratigraphy and implications for depositional history and tectonics of northern Tibetan Plateau. Earth Planet. Sci. Lett. 208, 253–269.
Wang, E., Xu, F.Y., Zhou, J.X., Wang, J.L., Burchfi, B.C., 2006. Eastward migration of the Qaidam basin and its implications for Cenozoic evolution of the Altyn Tagh fault and associated river systems. GSA Bull. 118, 349–365.
Wang, X.M., Qiu, Z.D., Li, Q., et al., 2007. Vertebrate paleontology, biostratigraphy, geochronology, and paleoenvironment of Qaidam Basin in northern Tibetan Plateau. Palaeogeogr. Palaeoclimatol. Palaeoecol. 254, 363–385.
Yang, P., Sun, Z.C., Li, D.M., Jing, M.C., Xu, F.T., Liu, H.M., 2000. Ostracoda extinction and explosion events of the Mesozoic–Cenozoic in Qaidam Basin, Northwest China. J. Palaeogeogr. 2, 69–74.
Yin, A., Nie, S., Craig, P., Harrison, T.M., Ryerson, F.J., Qian, X.L., Yang, G., 1998. Late Cenozoic tectonic evolution of the southern Chinese Tian Shan. Tectonics 17, 1–27.
Yin, A., Rumelhrt, P.E., Bulter, R., et al., 2002. Tectonic history of the Altyn Tagh fault system in northern Tibet inferred from Cenozoic sedimentation. GSA Bull. 114, 1257–1295.
Yin, A., Dang, Y.Q., Wang, L.C., Jiang, W.M., Zhou, S.P., Chen, X.H., Gehrels, G.E., McRivette, M.W., 2008. Cenozoic tectonic evolution of Qaidam basin and its surrounding regions (part 1): the southern Qilian Shan–Nan Shan thrust belt and northern Qaidam basin. GSA Bull. 120, 813–846.
Yue, L.P., Heller, F., Qui, Z.X., Zhang, L., Xie, G.P., Qiu, Z.D., Zhang, Y.X., 2001. Magnetostratigraphy and paleoenvironmental record of Tertiary deposits of Lanzhou Basin. Chin. Sci. Bull. 46, 770–774.
Yue, Y.J., Ritts, B.D., Graham, S.A., Wooden, J.L., Gehrels, G.E., Zhang, Z.C., 2003. Slowing extrusion tectonics: lowered estimate of post-Early Miocene slip rate for the Altyn Tagh fault. Earth Planet. Sci. Lett. 217, 111–122.
Zhao, Z.J., Fang, X.M., Li, J.J., 2001. Paleomagnetic dating of the Jiuquan Gravel in the Hexi Corridor: implication on the mid-Pleistocene uplift of the Qinghai–Tibetan Plateau. Chin. Sci. Bull. 46, 1208–1212.
Zheng, H.B., Powell, C.M., An, Z.S., Zhou, J., Dong, G.R., 2000. Pliocene uplift of the northern Tibetan Plateau. Geology 28, 715–718.
Zheng, D.W., Zhang, P.Z., Wan, J.L., Li, C.Y., Cao, J.X., 2003. Late Cenozoic deformation subsequence in northeastern margin of Tibet. Sci. China Ser. D Earth Sci. 46, 266–275.
Zhou, J.X., Xu, F.Y., Wang, T.C., Cao, A.F., Yin, C.M., 2006. Cenozoic deformation history of the Qaidam basin, NW China: results from cross-section restoration and implications for Qinghai–Tibet plateau tectonics. Earth Planet. Sci. Lett. 243, 195–210.
Zhu, L.D., Wang, C.S., Zheng, H.B., Xiang, F., Yi, H.S., Liu, D.Z., 2006. Tectonic and sedimentary evolution of basins in the northeast of Qinghai–Tibet Plateau and their implication for the northward growth of the Plateau. Palaeogeogr. Palaeoclimatol. Palaeoecol. 241, 49–60.
Zijderveld, J.D.A., 1967. A.C. demagnetization of rocks: analysis of results. Methods in Paleomagnetism, pp. 254–286.